Dynamic Wireless Power Transfer System for Electrical Vehicle Charging

Miguel Filipe Rodrigues de Melo, Instituto Superior Técnico

Abstract

Wireless charging electric vehicles (EV) during their traveling emerges as the new development trend in the EV field, as the onboard battery presents drawbacks such as a excess weight, long charging times and limited driving range.

Regarding this dissertation, it was intended to analyze and design a resonant converter to be used as a contactless charger for EVs.

Road irregularities, suspension height variations and the presence of external objects results in distances of 5 cm to 15 cm between primary and secondary transformer windings. In order to define the type of transformer core and windings to be used, a numerical characterization was performed of different transformers with low magnetic coupling.

Considering the low value of the magnetic coupling factor that this type of Energy transmission presents and the consequent impact on performance, a solution was studied using simulations to test various topologies of transformers with different windings distances, in order to obtain an adequate performance.

A series resonant converter was designed and its operation simulated, using different parameters: current to voltage phase difference, distance between primary/secondary and load. A three-phase rectifier was simulated to power one of the road resonant converters controlled by single pulse modulation (phase shift), using a series resonant compensation loop, and operating at a frequency of 85kHz.

1. Introduction

1.1. Motivation

The recent development of a diverse range of electric vehicles could revolutionize the paradigm of land mobility. In fact, this could have already happened if several constraints had not arisen, both in terms of construction, limited range, storage or energy conversion that made EV a non-viable option. However, due to the continuous increase of fossil fuel prices and all its inherent environmental consequences, the automotive market was forced to find new alternatives that would make it possible to mitigate this trend. The constant technological development in the area of power electronics allowed EVs to once again prove its potential as an increasingly viable alternative.

The need to improve energy efficiency is a reality, and here an opportunity arises for EVs to show their full potential and all their benefits for the world energy system. Combining this fact with the *smart-grid* concept, EVs with their low-emission, high-efficiency and low-noise characteristics are gradually becoming a very strong hypothesis in the automotive industry as the next-generation "green" vehicles.

Currently, EVs are not yet dominating the market due to some limitations, such as the high initial investment, poor charging infrastructures and limited battery range. However, this paradigm tends to change. For example, as of October 2020, the total number of Electric Vehicles (100% Electric and Plug-In Hybrids) sold in Portugal had already exceeded the number of the previous year. [1].

However, there are still some concerns about range and specifically about the next charging infrastructure. Having this two issues in mind, charging a vehicle while driving would mitigate both situations. In this sense, the motivation of this dissertation is precisely linked to the potential of developing a system that allows EV batteries to be dynamically charged along a stretch of road. This would allow for the reduction of the size of batteries, which would lead to an overall decrease in the EVs prices while increasing their range and reliability. Since Portugal has set 2040 as the deadline for stopping the sale of polluting (fossil fuel based) vehicles [2], this type of technology yet to be implemented and developed will be very important in the near future of electricity.

1.2. Objectives

The main objectives of this Msc. dissertation consists in a preliminary study of a contactless moving power transmission system, DWPTS (*Dynamic Wireless Power Transfer System*), along a road section: exploring the suitability of this technology for dynamic charging electric vehicles.

This being said, the fundamental objectives to be addressed in the dissertation will be:

- Design the proper power conversion topology;
- Dynamically model the involved subsystems;
- Numerically simulate the charging system;
- Design the closed loop charging process control system;
- Numerically evaluate the performance of the projected system in a closed loop;
- Evaluate the results obtained.

1.3. Document structure

This dissertation is divided into seven chapters, where the first serves as an introduction to the problem being analysed and the motivation that led to its choice.

In the second chapter, the *State of Art* is reviewed and all sub-components involved are explored from the introductory phase to component selection for the correct functioning of the system.

In the third chapter, the design of the resonant conversion topology is conceived.

In the fourth chapter, the modeling and simulation of the projected system is carried out, based on the second chapter and considering the interconnections between the different sub-systems involved: aiming for the best performance the elaboration of the closed loop control system of the charging sub-system will increased accuracy and reduced sensitivity to variations in process parameters (robustness) is developed. Computer simulations will be presented, using numerical values and components close to those used in a real EV.

In the fifth chapter, a numerical evaluation of the performance of the charging process resulting from the developed simulation is carried out, simultaneously comparing these same results with the theoretically predicted ones.

In the sixth and last chapter, the final conclusions of the work will be presented, making a general reflection on the results obtained, which could start a discussion of the introduction of this system in a real context. To conclude, final suggestions for improvement are presented for future work.

2. Theoretical Background

It is known that two of the biggest limitations when it comes to electric vehicles are range (dependent on the amount of energy stored in the battery) and the number (still relatively small) of battery charging stations. However, the dynamic mode of operation for EVs (DWPTS) is currently under development as an emerging technology. This method allows charging while the vehicle is in motion, requiring a smaller volume of battery storage, which is considered expensive, and therefore the range is significantly increased. However, a DWPTS faces several obstacles, including the following:

→ A considerable air-gap distance between the ground-vehicle pair (transmitter and receiver), affecting the coupling factor (k) of the coils;

→ Misalignment of the coils between transmitter and receiver, so that maximum energy transfer occurs through a magnetic field;

2.1. Wireless Energy Transfer Methods

Since the introduction of contactless charging systems for EVs, different technologies can be used to develop a WPTS, exploiting the properties of electromagnetic fields.

In recent times, however, interest has arisen in transferring energy at medium-high power to equipment at a certain distance. For these applications, DWPTS with resonant topology (also known as Resonant DWPTS) are used.

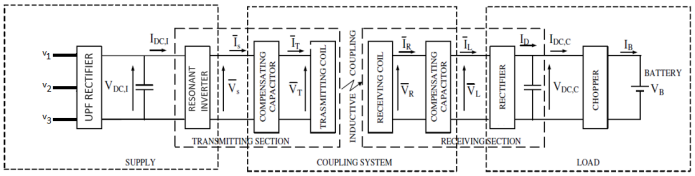

Figure 1: General scheme of a resonant DWPTS.

Compared to traditional inductive DWPTS, series and/or parallel compensation networks are added to the primary and secondary windings, not only to create the resonance case for greater energy transfer, but also to reduce additional losses. The resonance frequency, $f_{r(p,s)}$, is given by

$$f_{r(p,s)} = \frac{1}{2\pi\sqrt{L_{p,s} \cdot C_{p,s}}}, \tag{1}$$

When the resonant frequencies of the primary and secondary coils are equivalent, maximum power transfer occurs in the system. The operating frequency of the resonant DWPTS ranges from tens of kHz to several hundred kHz. By increasing the distance between the primary and secondary windings, the leakage flux, without a magnetic core, significantly reduces the mutual inductance and therefore reduces the coupling coefficient, (k).

The coupling coefficient value in resonant WPTS ranges from 0.2 to 0.3 due to the minimum height of the EVs, usually between 15–30 cm [3]. It is possible to apply (2) to calculate the coupling coefficient, k, where L_p and L_s are the self-induced transmitter and receiver coils, respectively. L_m is the mutual inductance between the two coils. If the primary and secondary coils are tightly coupled, the mutual inductance value would be greater and vice versa.

$$k = \frac{L_m}{\sqrt{L_p \cdot L_s}} \tag{2}$$

3. Resonant Conversion Topology Project

3.1. Resonant Meshes

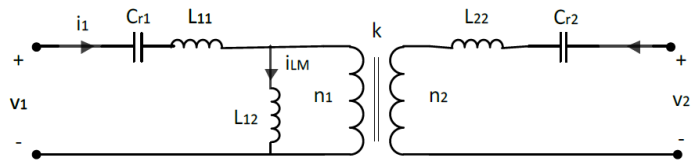

Figure 2: Series-Series Compensation.

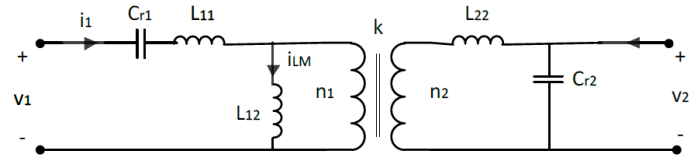

Figure 3: Series-Parallel Compensation.

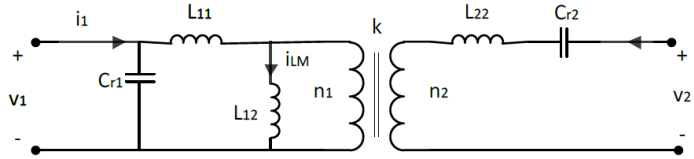

Figure 4: Parallel-Series Compensation.

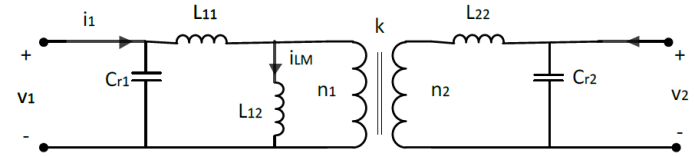

Figure 5: Parallel-Parallel Compensation.

3.2. Selection Process

In general, the four basic topologies are compared in the following five criteria that will allow for a good evaluation of the chosen choice:

- Maximum efficiency;
- Maximum power transferred to the load;
- The load-independent output voltage or output current;
- Compensation, independent of factor k;
- No magnetic coupling (k = 0);

The compensation method chosen was the Series-Series, which consists of placing a capacitor in series with the leakage inductance on the primary side, thus accomplishing the resonant mesh in series. Leakage inductances vary in a more restricted range of values, which makes this compensation more stable and predictable.

3.3. Transformer

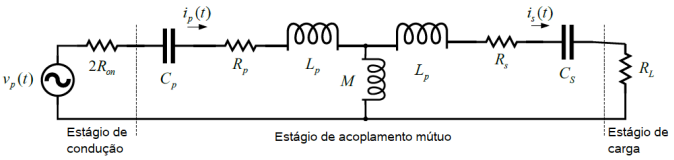

Figure 6: Equivalent Model of the WPTS Transformer.

3.3.1. Core Composition

The first approach adopted consisted of simulating and testing several ferrite cores, while varying the distance between primary and secondary (air-gap). For example, considering a frequency of 85 kHz, Figures (9-10) presents the simulation results of the magnetic flux lines through the calculation by *Finite Elements Method* (FEM), varying the distance between coils. Moreover, it is possible to observe in Figures (7-8) that the coil windings are found around the centerpiece, as well as the representative dimensions of the core used.

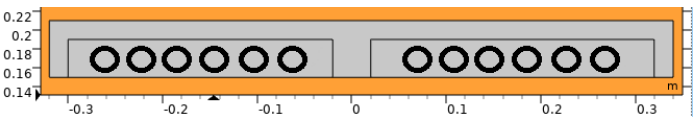

Figure 7: Section and dimensions of the top piece.

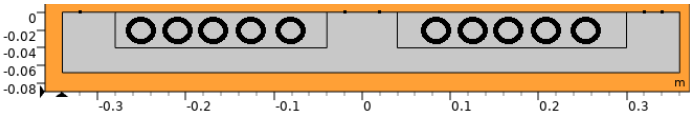

Figure 8: Section and dimensions of the lower piece.

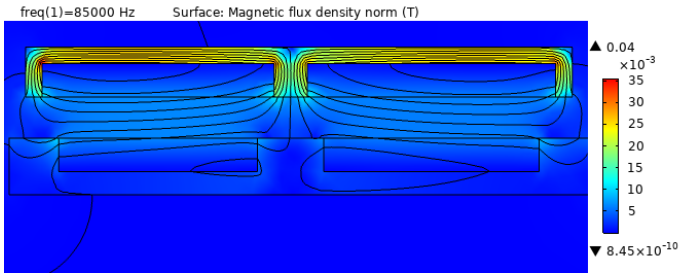

Figure 9: Simulation of an E-type Transformer, 5 cm apart.

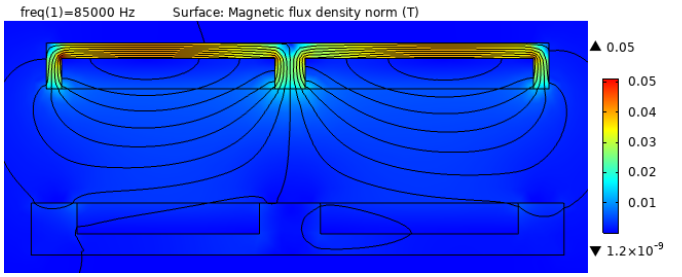

Figure 10: Simulation of an E-type Transformer, 15 cm apart.

The results reveal the distribution of magnetic flux for air-gaps that vary between 0 cm and 15 cm, showing that the distribution of the flux in the two situations weakens with the increase in the air gap, as expected.

4. Modeling the Contactless Power Transmission System

The main objective is based on the importance of using a resonant converter in order to improve the power transfer capacity of the charging system, using the principle of magnetic coupling.

During the pre-design of the system, it is necessary to take into account the fundamental initial parameters. The system specifications are described below:

- System working frequency of 85kHz;
- Power to be transferred, P = 50kW;
- For this application, taking into account the placement along the highways, considered communication routes that cover a large number of kilometers and knowing that the voltage to be used depends on the power level to be transferred, this will have to be considered High-Voltage, that is to say, the three-phase voltage source has an RMS voltage of 60kV and a frequency of 50Hz;
- Current Control Algorithm.

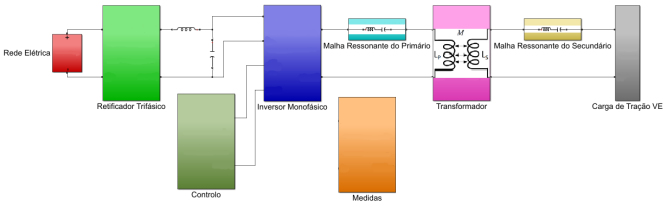

Figure 11: Simulation model implemented.

This converter is connected to the electrical grid (represented by non-ideal voltage sources) by means of a transformer which, at each secondary terminal (each phase), is connected to an inductive filter and then to a three-phase rectifier implemented downstream of the transformer. On the DC side, there is a capacitor whose function is to filter the voltage seen by the inverter.

4.1. Filter Coil - L_s

When introducing the inductive filter downstream of the transformer, the resulting simultaneous conduction phenomenon occurs causing the rectified voltage to be smaller due to the associated voltage drop, i.e, there will be a lower output DC voltage, $U_{2_{avmin}}$, given by [4]:

$$U_{2_{avmin}} = U_{2_{avs}} - \frac{p\omega L_s}{2\pi} \cdot I_{2_{av}} \tag{3}$$

Eventually, to maintain a target voltage of $U_{2_{avmin}} = U_{dc} = 700\text{V}$ DC, the value of V_M (shown below) will have to be increased in proportion to the voltage drop introduced by the inductive filter, which in turn depends on $U_{2_{avs}} = U'_{dc}$. This can be calculated, solving the equation (3) in order to $U_{2_{avs}}$,

$$U_{2_{avs}} = U_{2_{avmin}} + \frac{p\omega L_s}{2\pi} \cdot I_{2_{av}} = U'_{dc} \tag{4}$$

The filtering coil (L_s), is dimensioned taking into account the following expression [4]:

$$\cos(\epsilon + \gamma) = \cos\epsilon - \frac{\omega L_s I_{2_{av}}}{V_M \sin\left(\frac{\pi}{n}\right)} \tag{5}$$

Solving in order of L_s,

$$L_s = \frac{V_M \sin\left(\frac{\pi}{n}\right)(\cos\epsilon - \cos(\epsilon + \gamma))}{\omega I_{2_{av}}} \tag{6}$$

4.2. Control Design

For the control system, it was chosen to use linear controllers, consisting of proportional and integral (PI) compensators. The controller must guarantee closed-loop stability, reducing effect of disturbances and also ensure a fast, non-oscillating response, eliminating the static error.

Starting from the *Fourier* voltage series applied to this inverter,

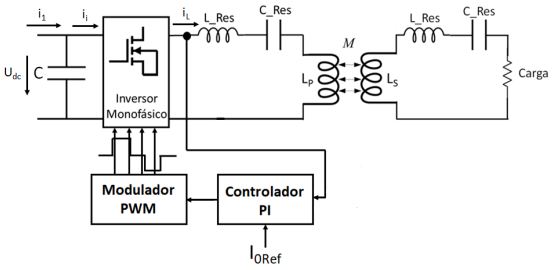

Figure 12: Illustration of the resonant power transfer control process.

$$u_2(t) = \sum_{n=1,3,5,..}^{\infty} \frac{4U}{k\pi} (\sin k\omega t) \tag{7}$$

The first harmonic associated with it, after development of the series, is given by:

$$U_{21RMS} = \frac{2\sqrt{2}U}{\pi} \sin\left(\frac{\delta}{2}\right) \tag{8}$$

The *Fourier* series associated with the current is obtained by dividing the *Fourier* series of the voltage by the RLC system impedance ($|Z_k|$,ϕ_k)

$$i_2(t) = \sum_{n=1,3,5,..}^{\infty} \frac{4U}{k\pi|Z_k|} (\sin k\omega t - \phi_k) \tag{9}$$

It is possible to obtain the RMS value of the current, associated with a certain gain (K_M) of the controller due to "U", which in turn allows to regulate the firing angle, δ,

$$i_{2_{ef}} = \frac{i_{2_{max}}}{\sqrt{2}} = \frac{\frac{4U}{\pi|Z_k|}}{\sqrt{2}} = G \times U_{21RMS} \tag{10}$$

where $\mathrm{G} = \dfrac{1}{|Z_1|}$

$$I_{21RMS} = \frac{\frac{2\sqrt{2}U}{\pi} \sin\left(\frac{\delta}{2}\right)}{\sqrt{R^2 + (\omega L)^2 + \left(\frac{1}{\omega C}\right)^2}} \tag{11}$$

To control the firing angle of the semiconductors, it is necessary to take into account the type of carrier wave in the modulation, in this case triangular. This being said, the carrier wave equation is defined in the frequency domain (ωt) as [4]

$$r(\omega t) = u_{cmáx} - \frac{u_{cmáx}}{\frac{\pi}{2}} \omega t \tag{12}$$

The angle, δ, is defined when the following condition is met: $\mathrm{r}(\omega \mathrm{t} = \dfrac{\pi}{2} - \dfrac{\delta}{2}) = u_c \sin(\omega \mathrm{t})$, that is,

$$u_{cmáx} - \frac{u_{cmáx}}{\frac{\pi}{2}} \left(\frac{\pi}{2} - \frac{\delta}{2}\right) = u_c \sin\left(\frac{\pi}{2} - \frac{\delta}{2}\right) \tag{13}$$

Assuming that, $\sin\left(\dfrac{\pi}{2} - \dfrac{\delta}{2}\right) \approx (\dfrac{\pi}{2} - \dfrac{\delta}{2})$, the angle, δ, can be expressed by

$$\delta \approx \frac{u_c}{u_{cmáx} + u_c} \cdot \pi \tag{14}$$

The chain-of-action gain, K_M, is obtained according to the following equation

$$K_M = \frac{\partial U_{21RMS}}{\partial u_c} \tag{15}$$

Returning to the first harmonic of the voltage, U_{21RMS} (8), and the value of, δ (14), it is possible to write the gain, K_M, as the derivative in function of the amplitude of the carrier wave:

$$K_M = (\sqrt{2}U) \cdot \frac{u_{cmáx}}{(u_{cmáx} + u_c)^2} \cdot \cos\left(\frac{\pi}{2} \cdot \frac{u_c}{u_{cmáx} + u_c}\right) \tag{16}$$

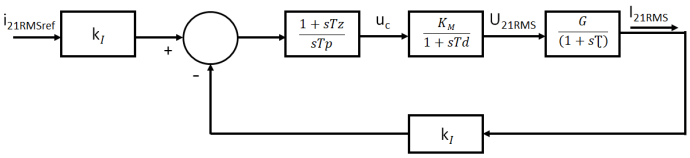

Figure 13: Current controller block diagram.

The RMS value was calculated by replacing the integral of the squared value with a low-pass filter (associated cut-off frequency: $\frac{fc}{10}$) in order to avoid the problem regarding the sliding mean initial value.

$$Td = Tz = \tau = \frac{1}{\frac{fc}{10}} \tag{17}$$

$$Tp = 4 \cdot \xi^2 \cdot Td \cdot G \tag{18}$$

Taking into account the previous expressions (17) and (18), it is possible to extract the following expressions from the proportional and integral gains of the PI compensators, knowing that the damping factor $\xi \in [0,1]$, where $\xi = 0$ corresponds to an undamped system and $\xi = 1$ corresponds to a critically dampened system. For calculation purposes, it was defined $\xi = \dfrac{\sqrt{2}}{2} = 0.7$

$$\begin{cases} Kp = \dfrac{Tz}{Tp} \\ Ki = \dfrac{1}{Tp} \end{cases} \tag{19}$$

5. Simulation of the Contactless Power Transmission System and Results Achieved

5.1. Electrical Grid + Transformer

Figures (14) and (15) show the waveforms of the phase to ground three-phase voltages and currents on the primary side of the transformer present in the *Electric Network* block.

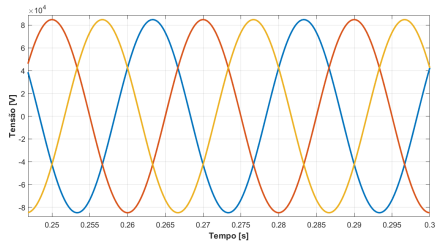

Figure 14: Representative three-phase voltages on the primary side of the transformer.

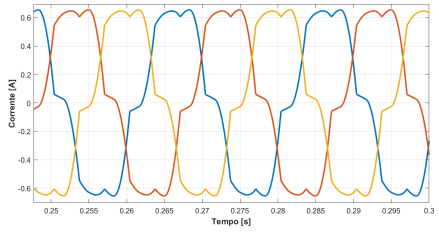

Figure 15: Three-phase currents representative of the primary side of the transformer.

Similarly, the waveforms of the phase to ground three-phase voltages and currents on the secondary side of the transformer are represented in Figures (16-17).

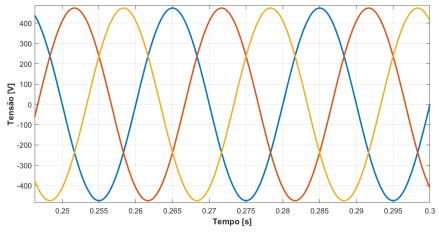

Figure 16: Representative three-phase voltages on the secondary side of the transformer.

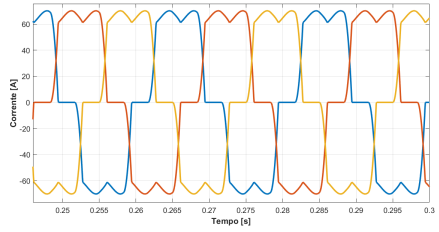

Figure 17: Three-phase currents representative of the secondary side of the transformer.

5.2. Filter Coil Influence - L_s

As stated in Chapter (4.1), the three-phase rectifier implemented downstream of the transformer, originates rectangular current waveform, which is not intended in Medium/High Voltage as it is considered harmful.

The introduction of a phase filtering coil, L_s, allows the feasibility of this type of rectifier in high voltage applications by removing the rectangular aspect, approaching an intended sine wave with a lower distortion rate.

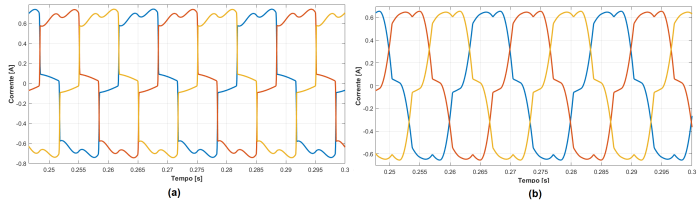

Figure 18: Comparison of primary currents: (a) - No coil, (b) - Presence of coil L_s.

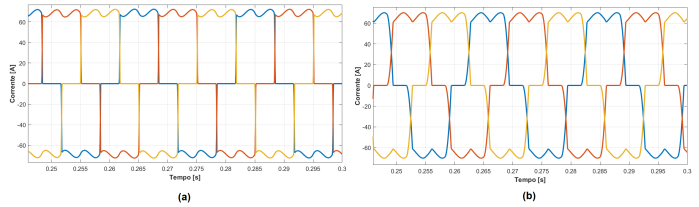

Figure 19: Comparison of secondary currents: (a) - No coil, (b) - Presence of coil L_s.

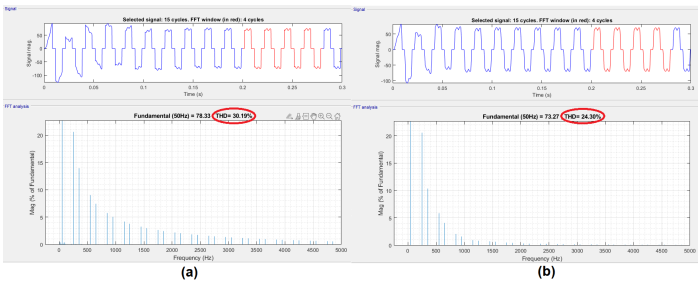

Figure 20: Comparison of the harmonic distortion rate of the secondary currents: (a) - No coil, (b) - Presence of the coil L_s.

5.3. Rectifier

In Figures (21-22) it is possible to observe the comparisons between Input/Output Voltages/Currents, which refer to the waveforms after rectification in the *Three-Phase Rectifier block* and consequent passage through the Filter LC represented in the general scheme of the converter (Figure (11)).

The capacitor (C) *shunt* will reduce the *ripple* associated with the voltage, but it will cause the diode current

to increase. This current can damage the diode and furthermore cause heating problems, decreasing the filter's efficiency. On the other hand, a coil (L) was used in series, reducing the maximum and RMS values of the output current and the output voltage.

The voltage stabilizing action of the capacitor *shunt* around, $U_{dc} = 700\,\text{V}$, not fully assuming this value due to the voltage drop present in the corresponding transformer impedance, and the smoothing action of the current present in the series coil can be observed in the following figures, with practically constant DC output.

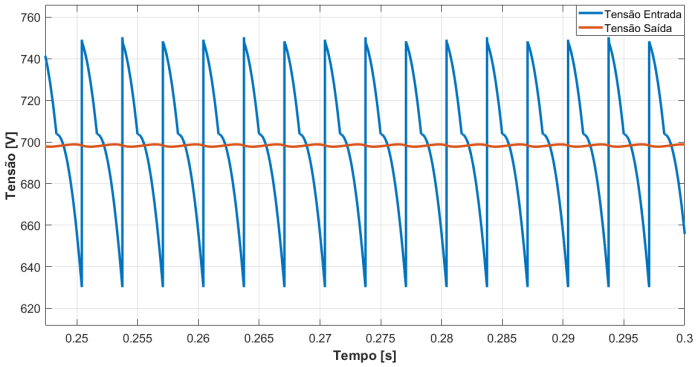

Figure 21: Waveforms of the voltage at the input of the filter LC after rectification and respective output voltage.

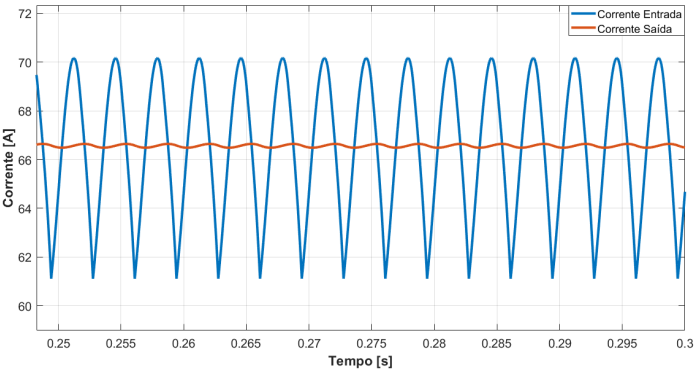

Figure 22: Waveforms of the current at the input of the filter LC after rectification and respective output current.

5.4. Modulator of the Resonant Inverter

As for the modulator, it works through a three-level sinusoidal pulse width modulation (*Single Pulse Modulation*).

In this type of modulation, there is only one output pulse per half cycle. The output is changed by varying the pulse width. The trigger signals are generated by comparing a sinusoidal reference (modulating wave) with a triangular reference (carrier) with a certain synchronization angular frequency (ωt).

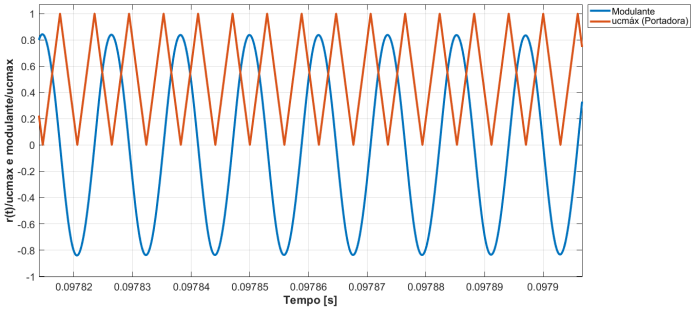

Figure 23: Waveforms, modulating and carrier.

Knowing that this is a three-level modulation, the functions f_{B1} and f_{B2} present in Figure (24) represent the state of the semiconductors associated with the 2 legs of the inverter where later, in Figure (25), the voltage associated with this type of modulation can be represented according to the following logic [4].

$$U_2 = (f_{B1} - f_{B2})U \longrightarrow f_{B1} - f_{B2} = \gamma \in [-1;1] \quad (20)$$

$$\gamma = \begin{cases} 1 \textbf{ if } f_{B1} = 1 \wedge f_{B2} = 0 \\ 0 \textbf{ if } \begin{cases} f_{B1} = 1 \wedge f_{B2} = 1 \\ f_{B1} = 0 \wedge f_{B2} = 0 \end{cases} \\ -1 \textbf{ if } f_{B1} = 0 \wedge f_{B2} = 1 \end{cases} \quad (21)$$

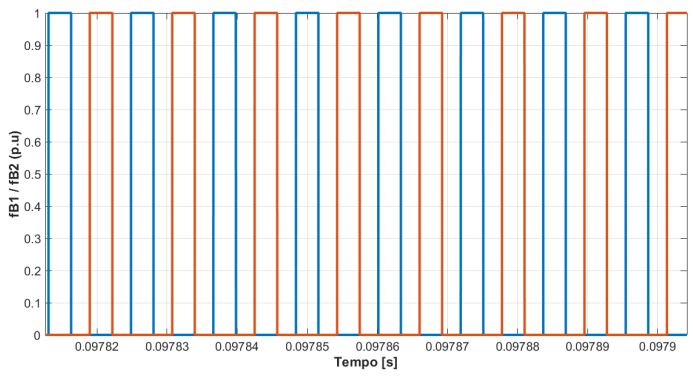

Figure 24: Characterization of the functions f_{B1} and f_{B2}, responsible for the alternating generation of impulses.

$$v_{PWM} = v_{S2} - v_{S3} = \gamma_1 U - \gamma_2 U = (\gamma_1 - \gamma_2)U \quad (22)$$

where, $\gamma = \gamma_1$ - $\gamma_2 \rightarrow \gamma \in$ {-1;0;1}

$$v_{PWM}(\gamma_1 - \gamma_2)U = \begin{cases} U \textbf{ if } \gamma_1 = 1 \wedge \gamma_2 = 0 \ (\gamma_2 = \text{NOT}(\gamma_1)) \\ 0 \textbf{ if } \begin{cases} \gamma_1 = 1 \wedge \gamma_2 = 1 \\ \gamma_1 = 0 \wedge \gamma_2 = 0 \end{cases} \quad (\gamma_2 = \gamma_1) \\ -U \textbf{ if } \gamma_1 = 0 \wedge \gamma_2 = 1 \ (\gamma_2 = \text{NOT}(\gamma_1)) \end{cases} \quad (23)$$

According to (22) and (23), it is possible to observe in Figure (25) the implementation of the voltage, v_{PWM}. This waveform has three levels in total, highlighting the functioning of the system in question.

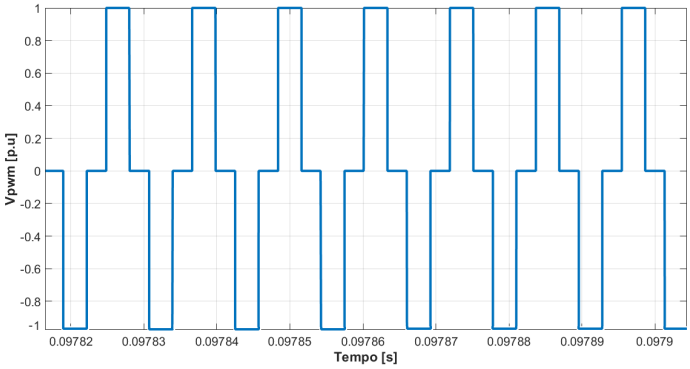

Figure 25: v_{PWM} 3 levels.

5.5. Resonant Inverter

5.5.1. 5cm distance between transmitter/receiver coils

The voltage and current waveforms in the series resonant circuit were measured. Figures (26) and (27) illustrate the *phase-shift* between the voltage on the primary and secondary sides of the circuit and show that the currents on each side are in phase with their corresponding voltages, which means that the transferred energy is considered mainly active, which was one of the main requirements. The caption regarding the inverter output voltage and its waveform confirm the theoretical model shown in the previous Figure (25).

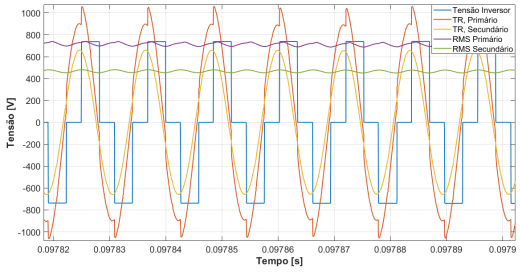

Figure 26: Waveforms of the voltages associated with the series resonant circuit.

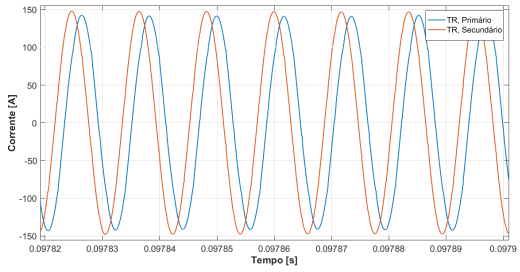

Figure 27: Waveforms of the currents associated with the series resonant circuit.

Interspersing the two previous figures, as mentioned throughout the dissertation, the intention in this type of systems is to guarantee that there are insignificant switching and conduction losses at the resonant frequency, reaching the *ZVS* and the *ZCS*.

As can be seen from Figure (28), the converter operating with a switching frequency, *fs*, below the resonance frequency, *fr*, switches in ZVS and ZCS.

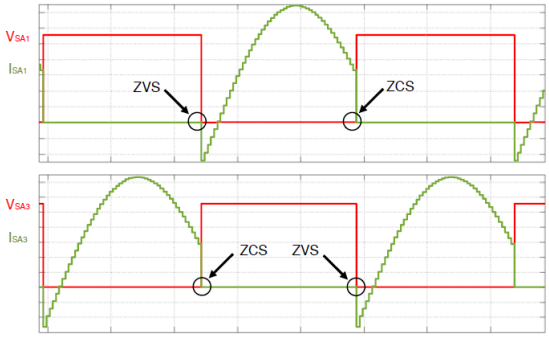

Figure 28: *Soft-Switching*, achieving *ZCS* and *ZVS*.

Regarding the current controller dimensioned in Chapter (4.2), Figure (29) illustrates the error between the applied current and the reference current. It is possible to observe correct reference value tracking with a small current ripple around the reference current. The error remains close to zero during the charging process.

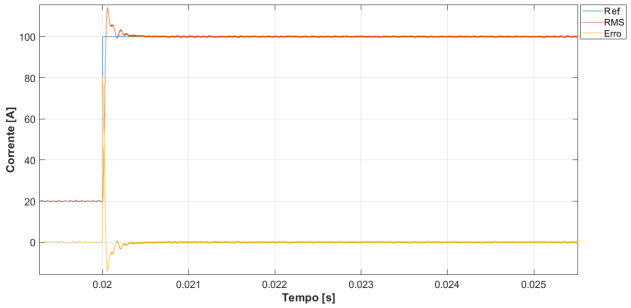

Figure 29: Applied (RMS) current, reference value (Ref) and associated error.

5.5.2. 15cm distance between transmitter/receiver coils

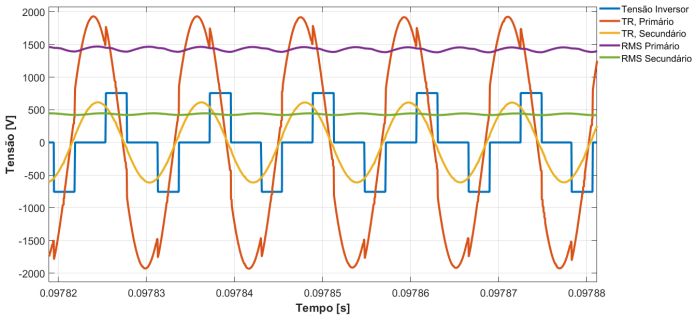

Figure 30: Waveforms of the voltages associated with the series resonant circuit.

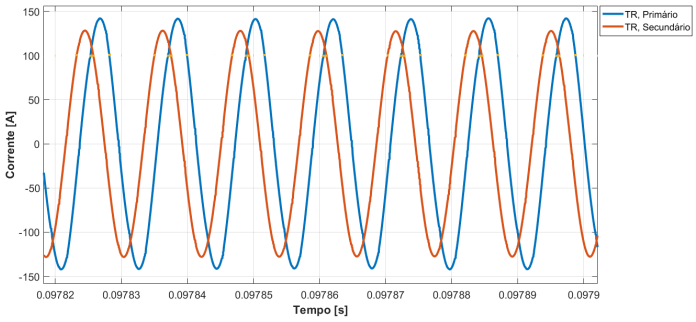

Figure 31: Waveforms of the currents associated with the series resonant circuit.

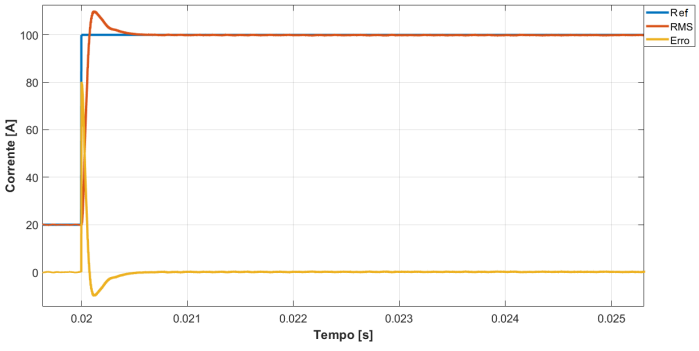

Figure 32: Applied effective current (RMS), reference value (Ref) and associated error.

5.5.3. Transferred Power

As discussed throughout the dissertation, Figures (33 - 34) show that the power to be transferred to the EV varies according to the air-gap distance present in the core of the transformer.

For a 5cm spacing (Figure (33)), it is slightly less than the power that the system was designed for, P = 50 kW, due to the inherent losses of the various elements of the system, even if *ZCS* and *ZVS* are performed on the devices.

For 15cm spacing (Figure (34)), as evidenced by the magnetic field leakage illustrated in Figure (10), the power transmitted to the EV decreases about 10 kW (P= 40 kW), which is due to the weak magnetic coupling existing between primary/secondary of the transformer, increasing the leakage inductances, L_{11} and L_{12}, decreasing the mutual inductance, L_{12}=L_M.

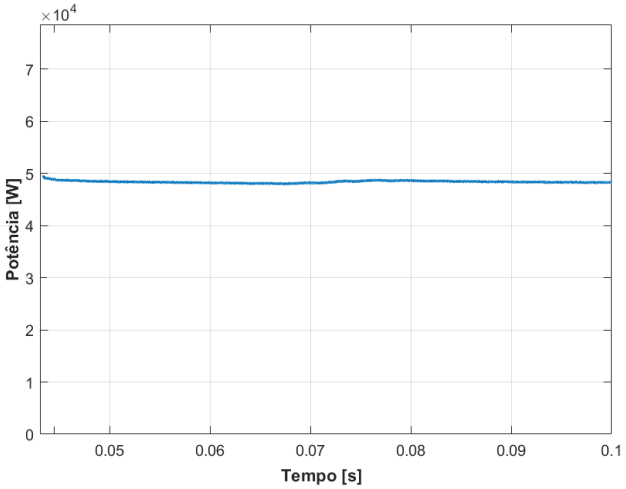

Figure 33: Power transferred by the resonant converter, d = 5cm.

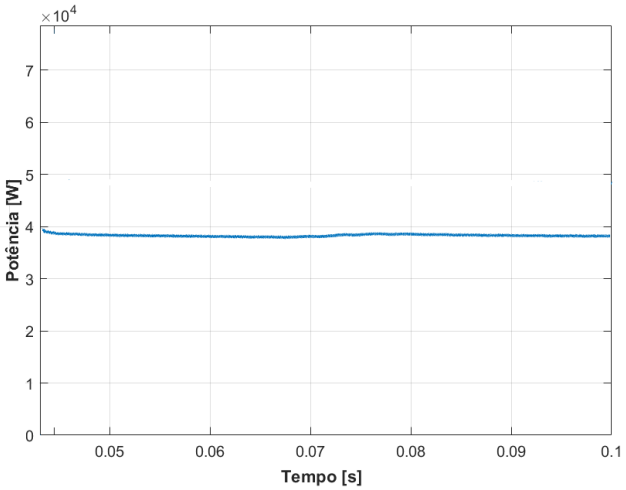

Figure 34: Power transferred by the resonant converter, d = 15cm.

5.5.4. Estimated Efficiency

In Figure (35), it is possible to observe the estimated value of the resonant converter efficiency from simulation (96%), from the input of the inverter to the vehicle's battery.

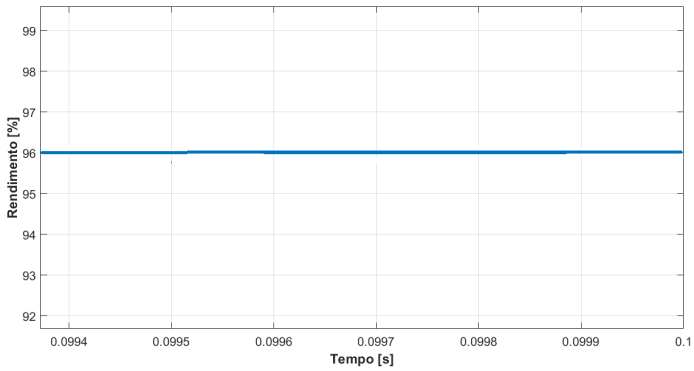

Figure 35: Estimated system efficiency.

After completing the simulation analysis of a series resonant converter, it can be concluded that the resonant and control topology proposed in the dissertation can work in electric vehicle applications.

The simulation of the non-contact charging prototype was essential to understand the working frequency limitations of the converters and the overall efficiency of the charging process using the selected compensation topology.

6. Conclusions and Future Work

6.1. Conclusions

The main objective of this dissertation was the implementation of a resonant converter that would allow the charging of electric vehicles without contact and in-motion, using a transformer with a low coupling factor, due essentially to the relationship between the air-gap distance and the dimensions of the core of the transformer. The implementation of this converter included the theoretical and practical application of the resonance principle, in which all reactive elements in the converter must be tuned to a given resonant frequency, in this case 85 kHz, allowing only the passage of the fundamental component of the current, leading to a greater amount of transferred energy.

Subsequent research led to the use of the equivalent three-parameter transformer model, an expedited equation model, which allowed us to obtain the output characteristics of the resonant converter operating with a weakly coupled transformer.

Through the simulations of the magnetic behavior of the transformer core, the characterizations carried out, as well as the results of electrical and electronic simulation, it was concluded that the coupling factor only depends on the magnetic properties of the transformer core, the geometry of the coils and the air-gap, being this study fundamental in the choice of the type of core to be used in this system.

The choice for the Resonant Converter to be applied in the system was the main result of Chapter (3). From the comparison between the possible resonant topologies, the series-series compensation was chosen. This type of compensation requires the operation of the Series Converter at working frequencies lower than the resonant frequency, allowing switching at zero current (ZCS).

After the mathematical analysis of the converter was completed, a theoretical simulation of a converter applied to an electric vehicle in a computational environment was carried out, which allowed for the observation of the behavior of the converter and the dynamics of the implemented controllers, which operated correctly through the application of a *phase-shift* modulation.

It is of utmost importance to experimentally materialize the resonant converter dimensioned during the work, in order to verify the validity of the obtained results. Due to time limitations, the experimental implementation was not carried out, however, the converter sizing methodology is presented, showing that it is a very efficient system with regard to energy transfer, enabling a power flow with a very high efficiency. It was also concluded that such a system must be used with high voltages and frequencies in order to obtain the best performance with the smallest dimension and lowest cost.

6.2. Future Work

To continue the work of this dissertation, some suggestions are presented below, with the main objective of improving the implemented system.

Regarding the simulations carried out to test the charger based on resonant power transfer principles, in addition to controlling the current, it would be beneficial to also control the power supplied to the load, thus a complete battery model could also be tested, making even more realistic when it comes to a contactless charger.

Regarding the air-gap distance, it is suggested to study the frequency variation of the inverter command such that this frequency is adapted to the variation of the resonant frequency, maximizing the transferred power.

Finally, it is suggested the construction and testing of a prototype charger for an electric vehicle, with power levels in the order of the values implemented in the simulation with possible development and implementation of fault diagnosis and fault tolerance algorithms in semiconductors and passive elements of the developed prototype;

References

[1] M. Nascimento. Vendas de Veículos Elétricos até outubro ultrapassam o total do ano passado. *Associação de Utilizadores de Veículos Elétricos*, 2020.

[2] G. André. Portugal: A partir de 2040 será proibida a venda de veículos poluentes novos. *Associação de Utilizadores de Veículos Elétricos*, 2018.

[3] D. Vilathgamuwa and J. Sampath. Wireless power transfer (wpt) for electric vehicles (evs)—present and future trends. In *Plug in electric vehicles in smart grids*, pages 33–60. Springer, 2015.

[4] J. F. A. da Silva. *Electrónica Industrial: Semicondutores e Conversores de Potência*. Fundação Calouste Gulbenkian, 2013.